JOURNAL OF CATALYSIS 117, 416–431 (1989)

Kinetic Analysis of the Oxidative Coupling of Methane over Na^+-Doped MgO

EIJI IWAMATSU AND KEN-ICHI AIKA[1]

Research Laboratory of Resources Utilization, Tokyo Institute of Technology, 4259 Nagatsuta, Midori-ku Yokohama, 227 Japan

Received October 25, 1988; revised January 13, 1989

The reaction rate of oxidative coupling of methane was studied kinetically using 0.0165 or 0.05 g of 15% Na^+–MgO catalyst at 923, 973, and 1023 K in a flow reactor under a CH_4 pressure of 1.36 to 13 kPa and an O_2 pressure of 0.36 to 4.7 kPa. The reaction rate was well expressed by the following mechanism. The kinetic data were analyzed by the Rideal-redox-type rate equation assuming methyl radical and active surface oxygen as the steady-state intermediates: (1) O_2 + site $\xrightarrow{2k_1}$ active oxygen, (2) CH_4 + active oxygen $\xrightarrow{k_2}$ $\cdot CH_3$ + OH(a) + site, (3) $\cdot CH_3 + xO \xrightarrow{k_3}$ CO, CO_2, (4) 2 $\cdot CH_3$ $\xrightarrow{k_4}$ C_2H_6. The constants k_1, k_2, x, and k_4/k_3^2 were obtained for every temperature. The activity is related to k_1 and k_2, while the selectivity (C_2/C_1) is related to k_4/k_3^2. The activation energies are 18 and 36 kcal/mol for k_1 and k_2, respectively. By considering the negative activation energy of k_3 (−7 kcal/mol), step 3 is inferred to contain the equilibrium reaction in which $\cdot CH_3$ and O_2 form methyl peroxide if the value of x is 2.0. The actual smaller value of x suggests that part of the methyl radical is oxidized by the surface oxygen. The specific surface area effect is also explained by this reaction mechanism if we assume that k_3 occurs on the surface (methyl peroxide decomposition) and k_4 occurs in the gas phase. The Langmuir–Hinshelwood mechanism can also be applied; however, it leaves several ambiguous points. These conclusions are only valid at high temperatures (923 to 1023 K) and under the low conversion (both X_{CH_4} and X_{O_2} are lower than 10%), whereas the consecutive oxidation of C_2 compounds should be taken into account under the high conversion condition.

INTRODUCTION

It has proved difficult to elucidate the complete mechanism of the oxidative coupling of methane ($2CH_4 + 0.5\ O_2 \rightarrow C_2H_6 + H_2O$, $2CH_4 + O_2 \rightarrow C_2H_4 + 2H_2O$) over catalysts because the reaction may involve gas phase radical chain mechanisms at high temperatures (a heterogeneous–homogeneous mechanism). However, it is very important to obtain the rate equations of this reaction for catalyst and reactor design. The rate equation should hopefully be related to the reaction mechanism, so that the rate constants are related to the catalytic properties and the transport phenomena.

The kinetic results obtained so far fall into two categories. The first is the Langmuir–Hinshelwood type involving the reaction of adsorbed methane and adsorbed oxygen; an example is the reaction over Sm_2O_3 (*1*). The second category is the redox type, involving the reduction of catalyst by CH_4 and the oxidation of it by O_2; an example is the reaction over BaO and PbO–Al_2O_3 (*2, 3*). The rate equations given in those reports treat only the rate of methane conversion and cannot explain the C_2 compound selectivity.

There are several reports in which each of the C_2 and C_1 compound formations is analyzed kinetically. Quite recently, Labinger and Ott (*4*) proposed a heterogeneous–homogeneous reaction mechanism in which the methyl radical is produced on the metal oxide surface, and the hydrocarbon is produced in the gas phase. They simulated their data, which was obtained by a

[1] To whom correspondence should be addressed.

0021-9517/89 $3.00

pulse method over Mn–MgO, by using their steady-state model. In this study we reach the same conclusion by a simple method using Na^+–MgO catalyst under steady-state conditions at various temperatures. Ali Emesh and Amenomiya derived the power rate law equation using the reaction over Bi_2O_3–K_2CO_3–Al_2O_3 (*5*). They calculated the reaction order of elementary steps in the reaction network (methane to CO_2, methane to C_2 hydrocarbons, and C_2 hydrocarbons to CO_2), where the mechanisms do not seem to agree completely with the rate equation.

For convenience, we start by proposing the following reaction scheme:

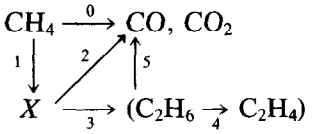

Although we did not detect *X* (the common intermediate of C_2H_6 and C_1 oxides) in this experiment, we assumed it to be $\cdot CH_3$, as has been observed over similar catalysts such as Li^+–MgO (*6*).

In general, the product ratio C_2/C_1 over effective catalysts is higher at higher temperatures when the reactions are compared under the same space velocity condition. If C_1 compounds (CO, CO_2) were formed exclusively through C_2 hydrocarbons (C_2H_6, C_2H_4) (steps 1–3–5 in the above scheme), the C_2/C_1 ratio should be low at a high temperature, where the conversion is higher than that at a low temperature. Therefore, C_1 oxides and C_2 hydrocarbons seem to be produced independently at the start of the reaction (steps 0, 1–2, and 1–3). In our previous study, we found that CO_2 production occurs at a lower temperature than that needed to produce C_2 hydrocarbons over the less effective catalysts (*7*). Over those catalysts (such as Mn^{2+}, Co^{2+}, Ag^+-doped MgO), the path of C_2 hydrocarbon production (steps 1–3) seems to be different from the path of C_1 oxide production (step 0). In the present work we refer to reaction mechanisms of that sort as the *independent reaction model*. On the other hand, over effective catalysts such as MgO catalysts doped with alkali metal oxides, C_2 hydrocarbons and C_1 oxides start to be produced at almost the same temperature (*7*). Thus, it seems probable that the production of C_2 hydrocarbons (steps 1–3) and C_1 oxides (steps 1–2) has a mutual intermediate (*X*). We refer to this type of reaction mechanism as a *reaction model with a common intermediate*. This mechanism is essentially the same as those proposed by Lunsford and colleagues (*6, 8*).

In the preceding paper, the effect of adding alkali metal to MgO was studied and was attributed to the two factors: chemical and physical (*7, 9–11*). Alkali increased the lattice distortion, which could cause an increase in surface active sites (chemical factor), and it also decreased the specific surface area of the catalyst (physical factor). Various materials that have been reported to be effective for this reaction (*1–36*) have low specific surface areas. For example, the surface areas of Li^+–MgO (*6, 14*), PbO–Al_2O_3 (*12, 13*), and Sm_2O_3 (*17*) are 8.9, 15, and 2 $m^2\ g^{-1}$, respectively. Although the effects of specific surface area are not discussed, a decrease of specific surface area has been observed when alkali or PbO metal was added. These physical factors must be derived from the reaction mechanism, which is related to the specific surface area.

In this work, the kinetics of oxidative coupling of methane over 15% Na^+–MgO (one of the most effective catalysts for this reaction) was studied to elucidate the mechanism and to obtain a suitable rate equation. The mechanism must explain several characteristics of the reaction, such as the high C_2 selectivity at high temperature and the specific surface area effect (physical factor).

To avoid the complexity of the algebraic treatment of rate equations, we often use the following approximation in this study:

$KP^i/(1 + KP^i)$ is replaced with KP^j $(0 < j < i)$, where P is the pressure and K, i, and j are the constants.

METHODS

Procedure

The catalyst preparation, the pretreatment, the flow reaction apparatus, and the analysis of reactants and products were the same as in our preceding work (*11*). To take the kinetic data, 0.0165–0.05 g of 15% Na^+–MgO catalyst was used. Up to 4 g of the catalyst was used to examine the catalyst weight/flow rate (W/F) dependence of the reaction. Since active materials are sometimes adhered to the reactor wall, blank runs were carried out to check that the wall reaction was negligible. C_2 hydrocarbons are defined as the sum of ethene and ethane, and C_1 oxides are defined as the sum of CO and CO_2. A very small amount of hydrogen was detected but not measured quantitatively.

W/F Dependence of the Reaction

As a preliminary, experimental runs with various W/F ratios were carried out by changing the catalyst weight under a total flow rate of 55 ml_{NTP}/min with 3.0 and 1.5 kPa of P_{CH_4} and P_{O_2} at 1023 K. The data obtained from the flow rate change sometimes differed from the data obtained from the weight change, probably because of the nature of the heterogeneous–homogeneous mechanism. No activity change was observed during the 3-h run for any sample. When more than 0.1 g of catalyst was used (W/F = 0.002 g min/ml), C_2 and C_1 production rates did not increase linearly, probably because of the remarkable O_2 pressure drop at the outlet of the reactor. However, it is interesting to note that the C_2/C_1 ratio is almost constant up to 0.3 g of catalyst (W/F = 0.006 g min/ml). This means that the production of C_2 hydrocarbons (steps 1–3) and C_1 oxides (steps 1–2) occur in a parallel way, and that formation of C_1 oxides from C_2 hydrocarbons (steps 5) would be neglected at the beginning of the reaction. The consecutive reaction path from C_2 hydrocarbons to C_1 oxides (step 5) seems to be important when catalyst weight is more than 0.5 g (W/F = 0.01 g min/ml). The O_2 conversion becomes almost 100% above 1 g of catalyst weight (W/F = 0.08 g min/ml). The ethene/ethane ratio increases from 0.1 g of catalyst (W/F = 0.002 g min/ml) to 4 g of catalyst (W/F = 0.08 g min/ml). Therefore, C_2H_4 seems to be a secondary product via C_2H_6 from CH_4. For comparison, oxidation of pure C_2H_6 was carried out both with 0.018 g of 15% Na^+–MgO and without catalyst at 1023 K. Table 1 shows the results. C_2H_4 was the main product in both runs. Note that the reaction does occur without the catalyst. The partial pressure of C_2H_6 at the blank run (no catalyst) was about 20 times higher than the partial pressure of C_2H_6 produced in the run with oxidative coupling. However, the ethane-to-ethene path (step 4) seems to proceed in the gas phase in the oxidative-coupling system at 1023 K.

Rate Measurement at Low Conversion under Various Temperatures and Pressures

The activity was measured by changing temperature, P_{CH_4}, and P_{O_2}. P_{CH_4} and P_{O_2} were controlled by changing the flow rate of

TABLE 1

Ethane Oxidation with and without Catalyst[a]

Product	Yield (%)	
	Blank (without catalyst)	15% Na^+–MgO[b]
CH_4	8.2	7.6
C_2H_4	54.3	54.1
CO	21.8	17.5
CO_2	0.7	2.9

[a] Reaction temperature was 1023 K; feed rates were as follows: C_2H_6 = 1.5 ml/min, air = 3.75 ml/min, He = 50 ml/min.

[b] Catalyst weight = 0.018 g.

CH_4, O_2, and He. The total flow rate was usually 55 ml_{NTP}/min (135 mmol/h). At a temperature of 923 K, 16 runs were carried out over 0.05 g 15% Na^+–MgO under a CH_4 pressure of 1.81 to 13.0 kPa and an O_2 pressure of 0.40 to 4.71 kPa. At 973 K, 15 runs were carried out over 0.0165 or 0.05 g of 15% Na^+–MgO under a CH_4 pressure of 1.36 to 13.0 kPa and an O_2 pressure of 0.36 to 3.98 kPa. At 1023 K, 15 runs were carried out over 0.0165 g of 15% Na^+–MgO under a CH_4 pressure of 1.36 to 13.0 kPa and an O_2 pressure of 0.36 to 3.98 kPa. The CH_4 and O_2 conversions were kept at less than about 10%. C_2 formation rates were 2.7 to 9.8 μmol/h at 923 K, 2.6 to 23.5 μmol/h at 973 K, and 12.6 to 53.2 μmol/h at 1023 K. C_1 formation rates were 37 to 299, 34 to 195, and 21 to 285 μmol/h, respectively. No significant deactivation was observed over several runs, and the activity did not change when the sample was replaced with another sample of the same batch.

RESULTS

Power Rate Law Expression

Of the 46 runs, some were carried out at constant CH_4 pressure or O_2 pressure to give the simple pressure dependence. Figure 1 shows the CH_4 and O_2 pressure dependences of the methane conversion rate over 15% Na^+–MgO at 1023 K. The reaction orders of CH_4 and O_2 for the methane conversion rate at 1023 K are 0.3 and 0.8, respectively. The reaction orders at 923 and 973 K were also obtained and are given in Table 2. The rate of total CH_4 conversion has an order of reaction between 0 and 1 for both methane and oxygen pressures. The same tendency has been found for the results over Sm_2O_3 (*1*) and BaO (*3*).

TABLE 2

Apparent Reaction Orders for R_{CH_4}, R_2, and R_1 on 0.0165 or 0.05 g 15% Na^+–MgO

	Order at 923 K		Order at 973 K		Order at 1023 K	
	CH_4	O_2	CH_4	O_2	CH_4	O_2
R_{CH_4}[a]	0.7	0.6	0.3	0.7	0.3	0.8
R_2[b]	1.3	−0.4	0.5	0.1	0.5	0.2
R_1[c]	0.7	0.7	0.3	0.9	0.3	1.0

[a] $2R_2 + R_1$ (rate of methane consumption).
[b] Rate of C_2 ($C_2H_6 + C_2H_4$) formation.
[c] Rate of C_1 ($CO + CO_2$) formation.

Figure 2 shows the formation rate of C_2 hydrocarbons and C_1 oxides over 15% Na^+–MgO at 1023 K as a function of the CH_4 and O_2 pressures. The reaction orders

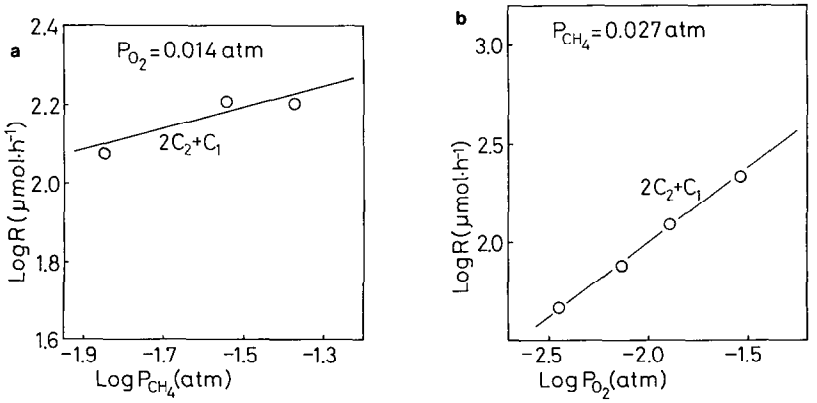

FIG. 1. CH_4 pressure dependence (a) and O_2 pressure dependence (b) for the methane conversion rate over 0.0165 g of 15% Na^+–MgO at 1023 K.

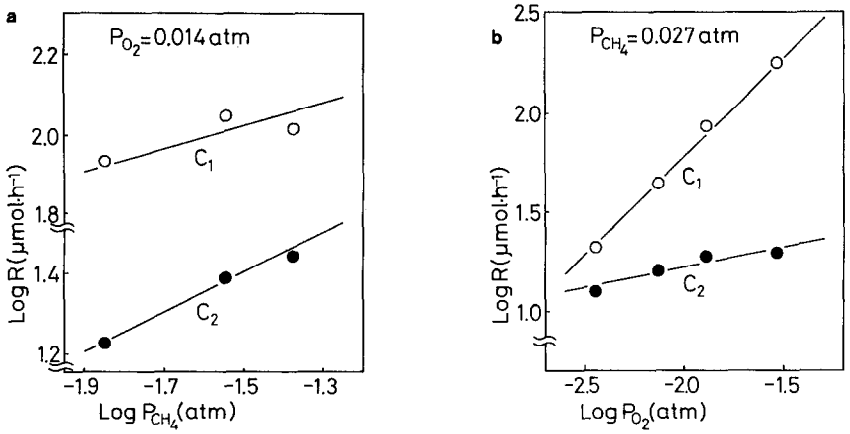

FIG. 2. CH_4 pressure dependence (a) and O_2 pressure dependence (b) for the C_2 and C_1 hydrocarbon formation rate over 0.0165 g of 15% Na^+–MgO at 1023 K.

of CH_4 and O_2 for the rate of C_2 and C_1 formation at the three temperatures are given in Table 2. At all three temperatures, the CH_4 pressure dependence for C_2 formation was higher than that for C_1 formation; this finding is related to the fact that 1 mol of C_2H_6 is produced from 2 mol of CH_4, whereas 1 mol of CO_2 is produced from 1 mol of CH_4. The O_2 pressure dependence for C_2 formation was lower than that for C_1 formation. The relation between these results and the reaction model is described in detail under Discussion.

Kinetic Simulation Based on the Rideal-Redox Mechanism

Several models are discussed in this work. First, we consider a mechanism referred to as the Rideal-redox mechanism, which is based on the following three assumptions. (i) The gas phase methyl radical ($\cdot CH_3$), which is expected to be the intermediate of this reaction, is produced from gas phase methane and adsorbed oxygen. (ii) The surface oxygen supplied from O_2 and consumed by CH_4 is at a steady state. (iii) $\cdot CH_3$ is converted to C_2H_6 by coupling and to CO_2 by oxidation, and it is also at a steady state. In the following reaction mechanism, [oxygen] indicates an active surface oxygen, and xO indicates the oxygen species that oxidize the methyl radical to CO_2. xO is a symbol of active oxygen which cannot be determined exactly at this moment. Afterward this is assumed to be the mixture of the gas phase O_2 (main species) and the surface oxygen (subspecies). Symbol xO is used so that the reader may easily note the kinetic expression. Secondary reactions from ethane to ethene or from ethene to CO, CO_2 are neglected because of the low conversion.

$$O_2 + \text{site} \xrightarrow{2k_1} [\text{oxygen}] \quad (1)$$

$$CH_4 + [\text{oxygen}] \xrightarrow{k_2} \cdot CH_3 + OH(a) + \text{site} \quad (2)$$

$$\cdot CH_3 + xO \xrightarrow{k_3} CO, CO_2 \quad (3)$$

$$2 \cdot CH_3 \xrightarrow{k_4} C_2H_6 \quad (4)$$

Equations (1) and (2) indicate a redox of surface oxygen (redox mechanism) and Eq. (2) indicates no adsorption of methane (Rideal mechanism). For simplicity and to conform with the previous report (*4*), in Eq. (1) the adsorption rate of O_2 is assumed to be proportional to the O_2 pressure and the concentration of the active site. If O_2

reacts with two sites, the rate should be proportional to square of the site, but at low concentrations of the adsorbed oxygen the two cases do not differ much. Therefore, we cannot decide the form of active oxygen, O(a) or O_2(a), here. By using a steady-state treatment for [oxygen] in Eqs. (1) and (2), the following equations are obtained, where θ is coverage of surface-active oxygen:

$$\frac{d\theta}{dt} = k_1 P_{O_2}(1 - \theta) - k_2 P_{CH_4}\theta = 0 \quad (5)$$

$$\theta = \frac{k_1 P_{O_2}}{k_1 P_{O_2} + k_2 P_{CH_4}}. \quad (6)$$

By using a steady-state treatment of $\cdot CH_3$ in Eqs. (2), (3), and (4), and substituting θ in these equations with Eq. (6), Eq. (7) is obtained. In this case, the oxidation rate of $\cdot CH_3$ is assumed to be proportional to $P_{O_2}^{x/2}$ in Eq. (3) and the meaning of x will be discussed later:

$$\frac{dP_{\cdot CH_3}}{dt} = \frac{k_1 P_{O_2} k_2 P_{CH_4}}{k_1 P_{O_2} + k_2 P_{CH_4}} - k_3 P_{\cdot CH_3} P_{O_2}^{x/2} - 2k_4 P_{\cdot CH_3}^2 = 0. \quad (7)$$

By resolving this equation, $P_{\cdot CH_3}$ is obtained:

$$P_{\cdot CH_3} = \frac{k_3 P_{O_2}^{x/2}}{4k_4} \left(\left(1 + \frac{8k_1 k_2 k_4 P_{O_2} P_{CH_4}}{k_3^2 P_{O_2}^x (k_1 P_{O_2} + k_2 P_{CH_4})}\right)^{0.5} - 1\right). \quad (8)$$

For convenience, we define

$$k_1 P_{O_2} = A \quad (9)$$

$$k_2 P_{CH_4} = B \quad (10)$$

$$\frac{k_4}{k_3^2 P_{O_2}^x} = C. \quad (11)$$

Then, the following two equations are obtained:

$$\frac{dP_{C_2H_6}}{dt} = R_2 = k_4 P_{\cdot CH_3}^2 = \frac{1}{16C}\left(\left(1 + 8C\frac{AB}{A + B}\right)^{0.5} - 1\right)^2 \quad (12)$$

$$\frac{dP_{CO_2}}{dt} = R_1 = k_3 P_{\cdot CH_3} P_{O_2}^{x/2} = \frac{1}{4C}\left(\left(1 + 8C\frac{AB}{A + B}\right)^{0.5} - 1\right). \quad (13)$$

In other words, the formation rates of C_2 compounds and C_1 oxides have been obtained as a function of P_{CH_4} and P_{O_2}.

C (Eq. (11)) can be obtained as $C = R_2/R_1^2$ by Eqs. (12) and (13). We multiplied the C_1 and C_2 formation rates obtained over 0.0165 g of catalyst at 973 and 1023 K by a factor of 0.05/0.0165 in order to compare the activity with the same catalyst weight. Figure 3 shows the values of C plotted as a function of P_{O_2} at the three temperatures, where the straight lines represent Eq. (11). It can be seen that the relations between C and P_{O_2} are independent of reaction temperature; that is, the order of P_{O_2} is -1.6 ($x = 1.6$). The reason for this result is discussed later. By using C and P_{O_2} for each data point, we calculated $CP_{O_2}^{1.6}$ (that is, k_4/k_3^2). The mean value of k_4/k_3^2 at each temperature is shown in Table 3. The rate of methane conversion is calculated as $2R_2 + R_1$, which gives $AB/(A + B)$ (from Eqs. (12) and (13)). Figure 4 shows $P_{O_2}(A + B)/AB = 1/k_1 + 1/k_2\,(P_{O_2}/P_{CH_4})$ plotted as a function of P_{O_2}/P_{CH_4}. The ordinate crossing gives $1/k_1$ and the slope gives $1/k_2$. The values of k_1 and k_2 obtained at each temperature are shown in Table 3. The temperature effect of k_1 and k_2 gives the activation energies (E_1 and E_2) of Eqs. (1) and (2): E_1 (the activation energy of the oxidation of the catalyst by O_2) is 18 ± 3

TABLE 3

Constants of the Reaction Rates on the Basis of the Rideal-Redox Mechanism[a]

	923 K	973 K	1023 K
k_1	0.152	0.162	0.39
k_2	0.079	0.23	0.53
k_4/k_3^2	0.76	1.77	1.57
x	1.60	1.60	1.60

[a] Values were rearranged per constant catalyst weight (0.05 g 15% Na^+–MgO). The units used were kPa and mmol/h.

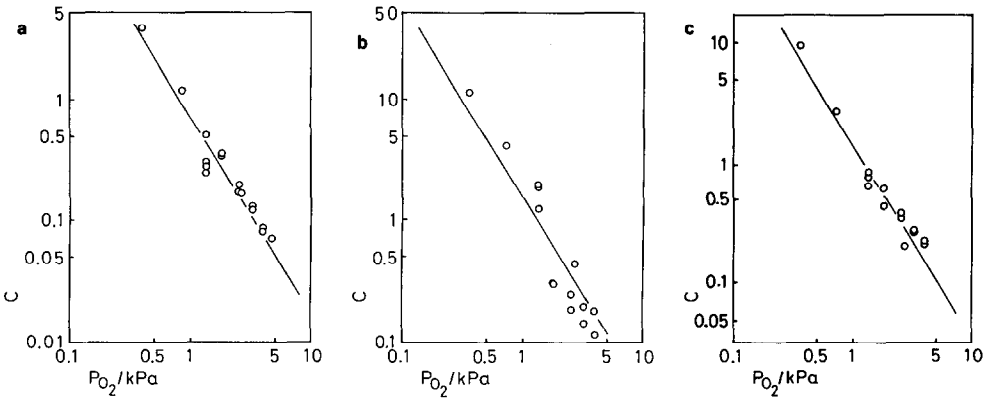

FIG. 3. O_2 pressure dependence for C over 0.05 g of 15% Na^+–MgO at 923 K (a), at 973 K (b), and at 1023 K (c). See text for C ($C = R_2/R_1^2$).

kcal mol^{-1}, and E_2 (the activation energy of the reduction of the catalyst by CH_4) is 36 ± 3 kcal mol^{-1}.

Kinetic Simulation based on the Langmuir–Hinshelwood Mechanism

In this section, we consider the so-called Langmuir–Hinshelwood mechanism, which involves the following assumptions. (i) The gas phase $\cdot CH_3$, an expected intermediate of this reaction, is produced by the reaction of adsorbed methane and adsorbed oxygen. (ii) $\cdot CH_3$ is converted to C_2H_6 by coupling and converted to CO_2 by oxidation, and the radical is at a steady state. We do not specify the form of adsorbed methane (CH_4(a)), of adsorbed oxygen (O*) that reacts with methane, or of oxygen (xO) that reacts with $\cdot CH_3$. The reaction mechanism including the tentative intermediates is

$$\tfrac{1}{2}O_2 \overset{K_0}{\rightleftharpoons} O^* \qquad (1a)$$

$$CH_4 \overset{K_m}{\rightleftharpoons} CH_4(a) \qquad (2'a)$$

$$CH_4(a) + O^* \overset{k_2}{\rightarrow} \cdot CH_3 + OH(a) \qquad (2a)$$

$$\cdot CH_3 + xO \overset{k_3}{\rightarrow} CO, CO_2 \qquad (3a)$$

$$2\cdot CH_3 \overset{k_4}{\rightarrow} C_2H_6. \qquad (4a)$$

Equations (1a) through (13a) in this section correspond to Eqs. (1) through (13) in the preceding section. Although θ_{O^*} and $\theta_{CH_4(a)}$ in Eqs. (1a) and (2'a) should be treated with the Langmuir–Hinshelwood type equation, $KP/(1 + KP)$, the Freundlich type, which is an approximation of the Langmuir–Hinshelwood type, is used for convenience:

$$\theta_{O^*} = K_0 P_{O_2}^p \qquad (5a)$$

$$\theta_{CH_4(a)} = K_m P_{CH_4}^q. \qquad (6a)$$

By assuming a steady state of $\cdot CH_3$ in Eqs. (2a), (3a), and (4a), and substituting θ_{O^*}, and $\theta_{CH_4(a)}$ with Eqs. (5a) and (6a), Eq. (7a) is obtained. The oxidation rate of $\cdot CH_3$ is assumed to be proportional to $P_{O_2}^{x/2}$:

$$\frac{dP_{\cdot CH_3}}{dt} = k_2\theta_{O^*}\theta_{CH_4(a)} - k_3 P_{\cdot CH_3} P_{O_2}^{x/2} - 2k_4 P_{\cdot CH_3}^2$$
$$= k_2 K_0 K_m P_{O_2}^p P_{CH_4}^q - k_3 P_{\cdot CH_3} P_{O_2}^{x/2} - 2k_4 P_{\cdot CH_3}^2 = 0. \qquad (7a)$$

By resolving this equation, $P_{\cdot CH_3}$ is obtained:

$$P_{\cdot CH_3} = \frac{k_3 P_{O_2}^{x/2}}{4k_4}\left(\left(1 + \frac{8k_2k_4K_0K_mP_{O_2}^pP_{CH_4}^q}{k_3P_{O_2}^x}\right)^{0.5} - 1\right). \qquad (8a)$$

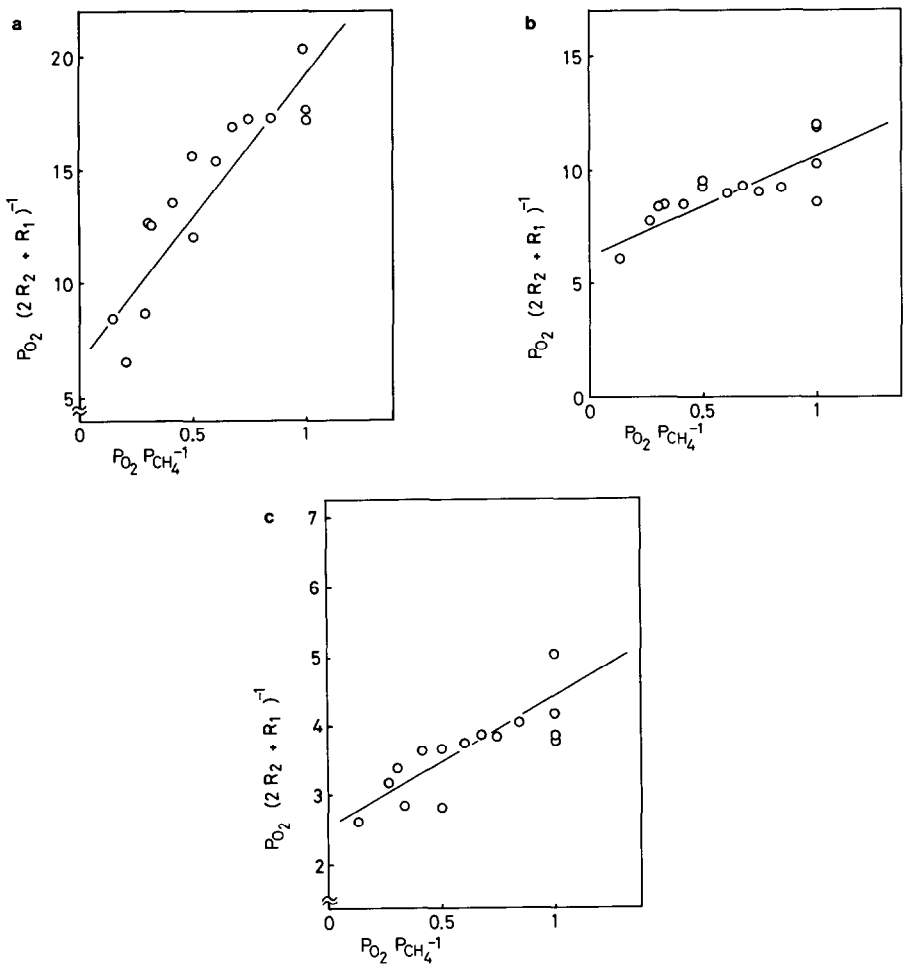

FIG. 4. $P_{O_2}/(2R_2 + R_1)$ as a function of P_{O_2}/P_{CH_4} over 0.05 g of 15% Na^+–MgO at 923 K (a), at 973 K (b), and at 1023 K (c). $(2R_2 + R_1)$ is identical to R_{CH_4} (rate of methane conversion). See text.

For convenience, the following two equations are defined:

$$K_0 P_{O_2}^p = A' \tag{9a}$$

$$K_m P_{CH_4}^q = B'. \tag{10a}$$

The formation rate of C_2 hydrocarbons and C_1 oxides is then obtained as follows, using A' and B' as well as C from Eq. (11),

$$\frac{dP_{C_2H_6}}{dt} = R_2 = k_4 P_{CH_3}^2 = \frac{1}{16C}\left(\left(1 + 8k_2A'B'C\right)^{0.5} - 1\right)^2 \tag{12a}$$

$$\frac{dP_{CO_2}}{dt} = R_1 = k_3 P_{\cdot CH_3} P_{O_2}^{x/2} = \frac{1}{4C}\left(\left(1 + 8k_2A'B'C\right)^{0.5} - 1\right). \tag{13a}$$

The values of C can be obtained as $C = R_2/R_1^2$ by Eqs. (12a) and (13a); i.e., the value of C in this model is identical to that for the Rideal-redox mechanism. Therefore, the order of P_{O_2} against C is also -1.6 ($x = 1.6$). Equations (12a) and (13a) give the relation $k_2A'B' = 2R_2 + R_1$, which can be calculated for each data point. By taking the loga-

TABLE 4

Constants of Reaction Rates on the Basis of the Langmuir–Hinshelwood Mechanism

	923 K	973 K	1023 K
p	0.55	0.66	0.76
q	0.68	0.33	0.27
$k_2K_0K_m$[a]	10.1	7.2	21.0
k_4/k_3^2	0.761	1.77	1.57
x	1.60	1.60	1.60

[a] Values were rearranged per constant catalyst weight (0.05 g of 15% Na^+–MgO). The units used were kPa and mmol/h.

rithms of $k_2A'B' = k_2K_0K_mP_{O_2}^pP_{CH_4}^q$ ($= 2R_2 + R_1$) as a function of log P_{O_2} and log P_{CH_4} with constant P_{O_2} or P_{CH_4}, p and q are calculated. The values of p and q are practically the same as the values of O_2 and CH_4 order in CH_4 conversion ($2R_1 + R_1$) in Table 2. The values at each temperature are listed in Table 4. It is thus seen that the experimental data can be also rearranged by the Langmuir–Hinshelwood mechanism.

Kinetic Simulation Based on the Multiple-Redox Mechanism

In the Rideal-redox mechanism, the reduction of the catalyst is assumed to be performed with CH_4 alone. In the multiple-redox mechanism, the reductant is assumed to be both CH_4 and $\cdot CH_3$. The other assumptions are the same as for the Rideal-redox mechanism. Equations (1), (2), and (4) are also applicable to this model, and xO from Eq. (3) is assumed to be identical with [oxygen]:

$$\cdot CH_3 + [\text{oxygen}] \xrightarrow{k_3} CO, CO_2. \quad (3b)$$

Now, by using the steady-state treatment for [oxygen] in Eqs. (1), (2), and (3b), Eqs. (5b) and (6b) are obtained. In this case, the rate of Eq. (1) is assumed to be proportional to $P_{O_2}^{0.5}$ (another case in which the rate of Eq. (1) is proportional to P_{O_2} will be described later):

$$\frac{d\theta}{dt} = k_1P_{O_2}^{0.5}(1 - \theta) - k_2P_{CH_4}\theta - k_3P_{\cdot CH_3}\theta = 0 \quad (5b)$$

$$\theta = \frac{k_1P_{O_2}^{0.5}}{k_2P_{CH_4} + k_3P_{\cdot CH_3} + k_1P_{O_2}^{0.5}}. \quad (6b)$$

By using the steady-state treatment for $\cdot CH_3$ in Eqs. (2), (3b), and (4) and substituting θ in Eq. (5b) with Eq. (6b), the following equation is obtained:

$$\frac{dP_{\cdot CH_3}}{dt} = k_2P_{CH_4}\theta - k_3P_{\cdot CH_3}\theta - 2k_4P_{\cdot CH_3}^2$$

$$= \frac{k_1k_2P_{O_2}^{0.5}P_{CH_4}}{k_2P_{CH_4} + k_3P_{\cdot CH_3} + k_1P_{O_2}^{0.5}} - \frac{k_1k_3P_{O_2}^{0.5}P_{\cdot CH_3}}{k_2P_{CH_4} + k_3P_{\cdot CH_3} + k_1P_{O_2}^{0.5}} - 2k_4P_{\cdot CH_3}^2 = 0. \quad (7b)$$

Therefore,

$$2k_3k_4P_{\cdot CH_3}^3 + 2k_4(k_1P_{O_2}^{0.5} + k_2P_{CH_4})P_{\cdot CH_3}^2 + k_1k_3P_{O_2}^{0.5}P_{\cdot CH_3} - k_1k_2P_{O_2}^{0.5}P_{CH_4} = 0. \quad (8b)$$

Equation 8b cannot be solved easily because the $P_{\cdot CH_3}$ term is third-order. Therefore, numerical calculations were performed to obtain $P_{\cdot CH_3}$ by assuming 27 cases for which each of the constant ratios k_1/k_4, k_2/k_4, and k_3/k_4 had values of 1, 10, and 100, respectively, in order to cover the wide conditions which cannot be expected a priori. At last, several practical values of P_{CH_4} and P_{O_2} were introduced in order to obtain $P_{\cdot CH_3}$ for the 27 cases. These hundreds values of $P_{\cdot CH_3}$ calculated can be used to obtain the rates of formation of C_2 hydrocarbons (by Eq. (12b)) and of C_1 oxides (by Eq. (13b)):

$$\frac{dP_{C_2H_6}}{dt} = R_2 = k_4P_{\cdot CH_3}^2 \quad (12b)$$

$$\frac{dP_{CO_2}}{dt} = R_1 = k_3P_{\cdot CH_3}\theta = \frac{k_1k_3P_{O_2}^{0.5}P_{\cdot CH_3}}{k_2P_{CH_4} + k_3P_{\cdot CH_3} + k_1P_{O_2}^{0.5}}. \quad (13b)$$

For every 27 cases, the rates of C_2 formation (R_2) were rearranged as a function of

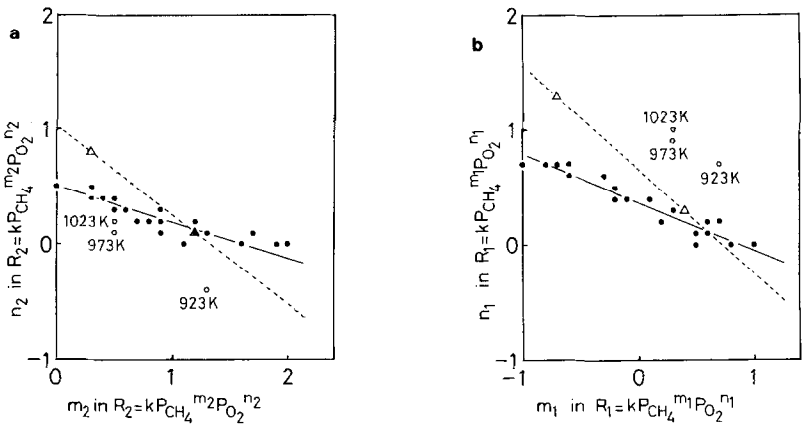

FIG. 5. (a) The relation between m_2 and n_2 (CH_4 order and O_2 order for C_2 production rate, see text). The value was calculated by assuming that the rate of Eq. (1) was proportional to $P_{O_2}^{0.5}$ (●) and to P_{O_2} (△). (○) Experimental values over 15% Na^+–MgO. (b) The relation between m_1 and n_1 (CH_4 order and O_2 order for C_1 production rate, see text). The value was calculated by assuming that the rate of Eq. (1) was proportional to $P_{O_2}^{0.5}$ (●) and to P_{O_2} (△). (○) Experimental values over 15% Na^+–MgO.

P_{CH_4} and P_{O_2} using the power rate law expression. The 27 sets of the P_{CH_4} and P_{O_2} dependences (represented to as m_2 and n_2) were found to have some relationship, $(\frac{2}{3}m_2 + 2n_2 = 1$, which is shown in Fig. 5a. For C_1 oxide formation, the rates R_1 were also rearranged into the power rate law expression. The 27 sets of P_{CH_4} and P_{O_2} dependences (represented to as m_1 and n_1) were also found to have a similar relation: $m_1 + \frac{8}{3}n_1 = 1$, this is shown in Fig. 5b.

As the second case, Eq. (1) was assumed to be first-order with respect to P_{O_2}. For this case, calculations similar to those above gave the relationships $\frac{2}{3}m_2 + n_2 = 1$ and $\frac{1}{2}(m_1 + 1) + \frac{2}{3}n_1 = 1$ (Figs. 5a and 5b).

The experimental data in Table 2 are also plotted in Figs. 5a and 5b. Clearly, these data do not obey either of the above two relationships. Therefore, it does not seem that this reaction can be explained by the multiple-redox mechanism model.

DISCUSSION

Rideal-Redox Mechanism

It was shown that the kinetic data over Na^+-doped MgO catalyst can be expressed by the rate equation based on the Rideal-redox mechanism. Sinev *et al.* have reported that the rate of CH_4 conversion (but not the rates of C_2 and C_1 formation) over $PbO–Al_2O_3$ is expressed by rate equations involving a CH_4–O_2 redox cycle (*2, 3*). They reported activation energies for MO (M = metal) reduction (Eq. (2)) of 31.5 ± 2.5 kcal/mol and for M oxidation (Eq. (1)) of 73.5 ± 3.5 kcal/mol. That means that the oxidation of catalyst proceeds preferably at higher temperature. In this study, we obtained an activation energy for MO reduction (on 15% Na^+–MgO) of 36 ± 3 kcal/mol and for M oxidation of 18 ± 3 kcal/mol. This means that the catalyst is more reduced or has more bare sites at higher temperatures, which seems reasonable. The simulated value of k_2 is lower than that of k_1 at 923 K, while that of k_2 is higher than that of k_1 at 1023 K.

What is the meaning of redox of the MgO catalyst (15% Na^+–MgO) used here? Since MgO itself is a stable oxide even at 1023 K, the reduction of MgO means the formation of coordinationally unsaturated Mg^{2+} ions on the surface. These surface Mg^{2+} ions would be covered by oxygen in the "oxidized state." Another explanation might be that Na^+ ions act as an oxygen reservoir

(for example $Na_2O + 0.5\ O_2 = 2\ Na^+O^-$, $Na_2O + 1.5\ O_2 = 2\ NaO_2$, or $Na_2O + 0.5\ O_2 = Na_2O_2$). However, we prefer the first model, in which MgO itself is the active center rather than the alkali ion as has been discussed in the previous paper (11).

What about the value of k_4/k_3^2, which is assumed to decide the selectivity of C_2 hydrocarbons against C_1 oxides? The results in Table 3 show that k_4/k_3^2 has a temperature coefficient of 14 kcal/mol. If Eq.(4) is a simple gas phase reaction of $\cdot CH_3$ combination, which has been reported to have a very low activation energy ($\simeq$0), the apparent activation energy of k_3 is -7 kcal/mol. This apparent negative activation energy of k_3 may be explained as follows. If O_2 is present, $\cdot CH_3$ is easily converted to $\cdot CH_3O_2$: this process is believed to be almost in equilibrium (Eq. (14)) (*37, 38*). We assume that CO_2 is mostly produced by decomposition of $\cdot CH_3O_2$. Now Eq. (3) (k_3) is assumed to be composed of

$$\cdot CH_3 + O_2 \overset{K_p}{\rightleftharpoons} \cdot CH_3O_2 \qquad (14)$$

$$\cdot CH_3O_2 \overset{k_{3a}}{\rightarrow} CO,\ CO_2. \qquad (14a)$$

Thus, k_3 is represented as $k_{3a}K_p$. Since ΔH for K_p has been reported to be -32 kcal/mol (*37, 38*), the apparent activation energy of k_{3a} is thus assumed to be 25 kcal/mol. At a high temperature, the equilibrium condition moves the system far to the left in Eq. (14). The ratio $\cdot CH_3O_2/\cdot CH_3$ is considered to be about 2% under the reaction conditions at 1023 K. Lunsford and colleagues have speculated that the similar mechanisms occur over Li^+–MgO and Na^+–CaO catalysts (*6, 39*).

If Eqs. (14) and (14a) only govern CO_2 formation, the value of x in Eq. (3) must be 2. Since the experimental value obtained is not 2 but 1.6, another path must also occur, for example the reaction of $\cdot CH_3$ with the surface:

$$\cdot CH_3 + \text{surface oxide}(O^{2-}) \rightarrow \text{methoxide(a)} \rightarrow CO_2. \qquad (15)$$

Although there are some ambiguous points, such that x is not 2, which suggest some contribution of Eq. (15), the Rideal-redox mechanism seems to be the most adequate mechanism and useful for the discussion of the C_2/C_1 selectivity.

Sinev *et al.* recently proposed a very similar treatment(*40*). In their work, the rate of C_1 formation is proportional to the square of methyl peroxide concentration, while it is first-order in our treatment.

Langmuir–Hinshelwood Mechanism

The kinetic data obtained over 15% Na^+–MgO could also be explained by using the Langmuir–Hinshelwood mechanism. Here we have to check the meaning of the rate constants. As shown in Table 4, $k_2K_0K_m$ does not seem to depend much on the reaction temperature. The value of k_2 is clearly higher at higher temperatures, because it is the rate constant of Eq. (2a). However, K_0 and K_m are clearly lower at high temperatures, because they are the adsorption equilibrium constants. As a result, $k_2K_0K_m$ is relatively constant in the temperature range 923 to 1023 K. We cannot derive individual values for k_2, K_0, and K_m by this method. Thus, this approach gives less information than the Rideal-redox mechanism.

From the nature of the adsorption equilibrium in Eqs. (5a) and (6a), the values of p and q must be higher (weak adsorption) at higher temperatures. However, although the value of p is higher at the higher temperatures, the value of q is not. Note that the value of p is greater than 0.5, indicating that oxygen should be adsorbed as the molecular species, O_2(a), instead of as the atomic species, O(a). This result is very similar to the results for the rate of CH_4 oxidation over several catalysts, for example, Sm_2O_3 (*1*), where the active oxygen species was reported to be O_2(a). At present, it is hard to decide the form of active oxygen. This model also can give the information about C_2/C_1 selectivity in a simple form. Overall, the Langmuir–Hinshelwood mechanism

leaves several ambiguous points, although it can be applied numerically.

Pressure Dependence

Our kinetic data were well expressed by the rate equation based on the Rideal-redox mechanism. The rate equations (Eqs. (12) and (13)) may be rewritten using a constant $x = 1.6$ as

$$\frac{dP_{C_2H_6}}{dt} = R_2 = \frac{k_3^2 P_{O_2}^{1.6}}{16k_4} \left(\left(1 + \frac{8k_1k_2k_4P_{O_2}P_{CH_4}}{k_3^2P_{O_2}^{1.6}(k_1P_{O_2} + k_2P_{CH_4})}\right)^{0.5} - 1\right)^2 \quad (12c)$$

$$\frac{dP_{CO_2}}{dt} = R_1 = \frac{k_3^2 P_{O_2}^{1.6}}{4k_4} \left(\left(1 + \frac{8k_1k_2k_4P_{O_2}P_{CH_4}}{k_3^2P_{O_2}^{1.6}(k_1P_{O_2} + k_2P_{CH_4})}\right)^{0.5} - 1\right). \quad (13c)$$

The sum of $R_1 + 2R_2$ gives $-d\mathrm{CH_4}/dt$, which leads the rate of CH_4 conversion, as

$$-\frac{dP_{CH_4}}{dt} = \frac{k_1P_{O_2}k_2P_{CH_4}}{k_1P_{O_2} + k_2P_{CH_4}}. \quad (16)$$

We then tried to transform the Eqs. (12c), (13c), and (16) to the power rate form using an approximation method, in order to compare the experimental data of power rate form. Table 5 shows the results. The orders in Table 5 are given as ranges because they were calculated by an approximation. Note that the CH_4 power in C_2 formation is higher than the CH_4 power in C_1 formation, because 1 mol of C_2 is formed by 2 mol of $\cdot CH_3$. It is also interesting to note that the O_2 order in C_2 formation can be negative. Indeed, the data at 923 K give a negative order (−0.4 in Table 2). A negative order is also seen on $SrCO_3$ (*41*). Similar results were reported by Ito *et al.* (*6*) and Hinsen *et al.* (*13*). Our experimental values (Table 2) are all within the range of the calculated values (Table 5). Therefore, the results of the power rate form are well explained by the Rideal-redox mechanism.

TABLE 5

Reaction Orders for R_{CH_4}, R_2, and R_1 Calculated on the Basis of the Rideal-Redox Mechanism on 0.0165 or 0.05 g of 15% Na^+–MgO at 923 to 1023 K

	Order	
	CH_4	O_2
R_{CH_4}[a]	0–1	0–1
R_2[b]	0–2	−1.6–1
R_1[c]	0–1	0–1.3

[a] $2R_2 + R_1$ (rate of methane consumption).
[b] Rate of C_2 hydrocarbon formation.
[c] Rate of C_1 oxide formation.

Possible Independent Path to CO_2

So far we have analyzed three reaction models that assume a common intermediate to both C_2 and C_1 compounds. This assumption was based on the fact that C_2 hydrocarbons and CO_2 start to form at the same temperature over the Na^+–MgO catalyst (*7*). Now we discuss the possibility of an independent path to CO_2 (step 0 in the initial scheme) from a kinetic viewpoint. As a matter of convenience, we assume that C_2 hydrocarbons are formed as in the Rideal-redox mechanism (Eqs. (1), (2), and (4)). However, Eq. (3) is replaced by the reaction

$$CH_4 + [\text{oxygen}] \rightarrow CO, CO_2 \quad (3c)$$

Thus, assuming that the concentration of surface [oxygen] is identical to θ in Eq. (6) and using the steady-state treatment for $\cdot CH_3$ in Eqs. (2) and (4), the following equations are obtained:

$$\frac{dP_{\cdot CH_3}}{dt} = \frac{k_1P_{O_2}k_2P_{CH_4}}{k_1P_{O_2} + k_2P_{CH_4}} - 2k_4P_{\cdot CH_3}^2 = 0 \quad (7c)$$

$$\frac{dP_{C_2H_6}}{dt} = R_2 = k_4P_{\cdot CH_3}^2 = \frac{k_1k_2P_{O_2}P_{CH_4}}{2(k_1P_{O_2} + k_2P_{CH_4})}. \quad (12d)$$

The rate of CO_2 formation (Eq. (3c)) is inde-

pendent of C_2 formation. It should be described as

$$\frac{dP_{CO_2}}{dt} = R_1 = k_3 P_{O_2}^{y} P_{CH_4}^{z}. \quad (13d)$$

This model suggests that any orders with respect to P_{CH_4} and P_{O_2} should be positive for C_2 or the CO_2 production rate. However, as shown in Table 2, the experimental results sometimes give negative orders with respect to P_{O_2} for C_2 hydrocarbon formation. Therefore, this reaction model is not applicable to the reaction over Na^+–MgO at higher temperatures. However, if the reaction is performed at low temperatures especially over transition-metal-doped MgO, the surface reaction to give CO_2 by way of surface methoxide may be important (*42*).

It has been pointed out that the CH_4 order for C_2 hydrocarbon formation is higher than that for C_1 oxides in any model with a common intermediate. The results in Table 2 show this tendency, which results from the fact that 2 mol of $\cdot CH_3$ give 1 mol of C_2H_6, whereas 1 mol of $\cdot CH_3$ gives 1 mol of C_1 oxides. On the other hand, this constraint does not hold for the independent reaction model. Since all $\cdot CH_3$ reacts to give C_2 hydrocarbons in this model, the CH_4 order for C_2 formation is between 0 and unity (Eq. (12d)), and the CH_4 order for C_1 oxide formation (z) is also between 0 and unity. Thus, CH_4 orders seem to be much the same in the two rate equations. In this sense, this model does not agree with the experimental results (Table 2).

Effect of Specific Surface Area on Selectivity

It has been shown that among MgO catalysts doped with various elements, catalysts with low specific surface area have higher C_2 selectivity at a similar conversion level (about 100% O_2 conversion). It has been suggested that this fact is due to the heterogeneous–homogeneous reaction mechanism (*7, 10, 11*). In this section, the surface area effect will be discussed through the Rideal-redox mechanism. We

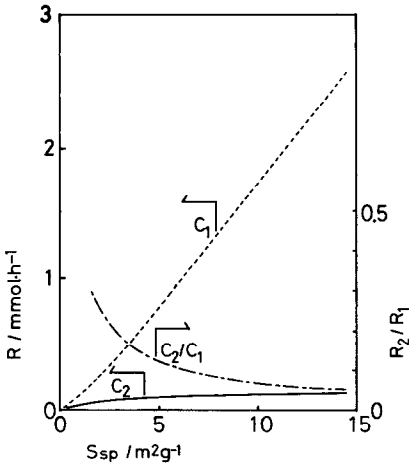

FIG. 6. R_2 (rate of C_2 hydrocarbon formation), R_1 (rate of C_1 oxide formation), and R_2/R_1 as a function of S_{sp} (specific surface area) for a constant catalyst weight (0.05 g). One point is a real datum (1023 K, P_{CH_4} = 2.72 kPa, P_{O_2} = 1.36 kPa, S_{sp} = 2 m^2 g^{-1}, W = 0.05 g).

consider the rate ratio of C_2 hydrocarbons to C_1 compounds, R_2/R_1, which is derived by Eqs. (9) to (13):

$$\frac{R_2}{R_1} = \frac{1}{4}\left(\left(1 + \frac{8k_1k_2k_4P_{O_2}P_{CH_4}}{k_3^2 P_{O_2}^{x}(k_1P_{O_2} + k_2P_{CH_4})}\right)^{0.5} - 1\right). \quad (17)$$

If all processes (Eq. (1) to (4)) are surface reactions, R_2/R_1 does not depend on the specific surface area, S_{sp}. If any process is not a surface reaction; however, R_2/R_1 could be a function of S_{sp}. If the $\cdot CH_3$ coupling process (k_4) is a gas phase reaction and the CO_2 formation process (k_3) needs the surface (probably through Eq. (14a)), then k_1, k_2, and k_3 are proportional to S_{sp}, but k_4 is independent of S_{sp}. In this case, R_2/R_1 changes as a function of S_{sp} as predicted by Eq. (17). The value of R_2/R_1 is higher at low S_{sp}. By Eqs. (12c) and (13c), R_2 and R_1 can also be expressed as functions of S_{sp}.

Suppose we could make various catalysts have the same chemical properties but different specific surface areas (S_{sp}). Figure 6 demonstrates how the production rates (R_2,

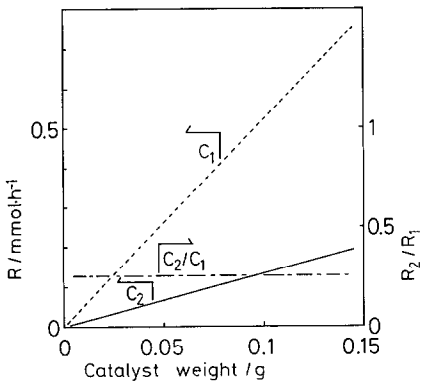

FIG. 7. R_2 (rate of C_2 hydrocarbon formation), R_1 (rate of C_1 oxide formation), and R_2/R_1 as a function of catalyst weight for constant S_{sp} (2 m^2 g^{-1}). One point is a real datum (1023 K, P_{CH_4} = 2.72 kPa, P_{O_2} = 1.36 kPa, S_{sp} = 2 m^2 g^{-1}, W = 0.05 g).

R_1) and selectivity (R_2/R_1) would change if we could change S_{sp} at a constant catalyst weight and volume. These results are based on the above assumptions and the kinetic data at one point (1023 K, P_{CH_4} = 2.72 kPa, P_{O_2} = 1.36 kPa, S_{sp} = 2 m^2 g^{-1}, W = 0.05 g). R_1 is almost proportional to S_{sp}, but R_2 gradually approaches saturation. R_2/R_1 is higher when S_{sp} is small. In this calculation, the value at S_{sp} = 2 m^2 g^{-1} is the only real value from the experiment.

Next, we suppose that the secondary reaction (C_2 to C_1 oxides) and reactant pressure drop could be neglected even at high conversion (high W/F). Thus, R_2 and R_1 are proportional to the catalyst weight (or contact time), and R_2/R_1 is independent of the catalyst weight. Figure 7 shows this relation: R_2, R_1, and R_2/R_1 as a function of the catalyst weight (W) where S_{sp} of the catalyst (2 m^2 g^{-1}) and the total flow rate (F = 55 ml/min) are constant. The value of 2 m^2 g^{-1} is the real value of S_{sp} for the 15% Na^+–MgO catalyst used in this reaction. R_2 and R_1 reach values where O_2 conversion would be 100% at some catalyst weight. By assuming the above method, R_2, R_1, and the catalyst weight that gives 100% O_2 conversion were calculated for various catalysts having various S_{sp}. The results are shown as a function of S_{sp} in Figs. 8a and 8b. When S_{sp} is high, a smaller weight of catalyst gives 100% O_2 conversion. As shown in Fig. 8a, the catalyst with S_{sp} = 0.3 m^2 g^{-1} achieves 100% O_2 conversion at a 2-g catalyst weight. To compare these calculations to the practical data, R_2/R_1 was calculated for 2 g of catalyst with various S_{sp} (Fig. 8b). In Fig. 8b, for S_{sp} less than 0.3 m^2 g^{-1}, the reactions are progressive; that is, R_2 increases with increasing S_{sp} as long as O_2 conversion is less than 100%. However, O_2 conversion reaches 100% at S_{sp} = 0.3 m^2

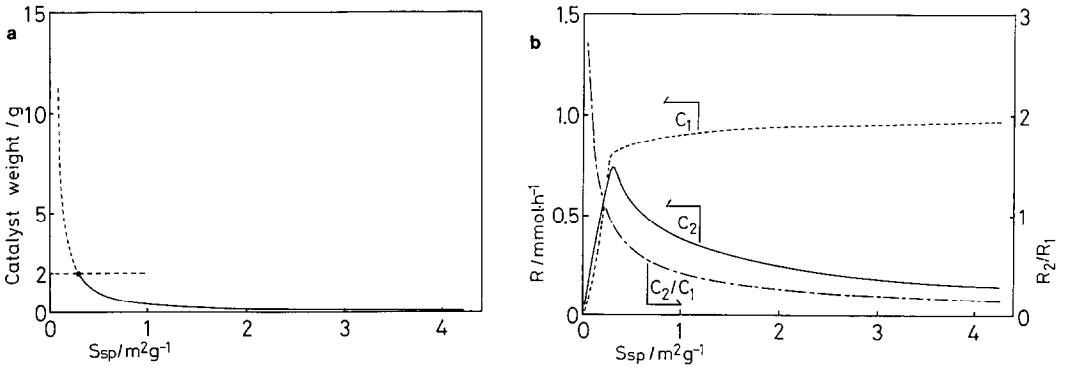

FIG. 8. (a) The catalyst weight necessary to get 100% O_2 conversion as a function of S_{sp} (1023 K). Reactant pressure drop and secondary reactions are neglected (see text). (b) R_2, R_1, and R_2/R_1 over 2 g of catalyst with various S_{sp} (1023 K). The value for $S_{sp} > 0.3$ m^2/g is calculated at 100% O_2 conversion. Reactant pressure drop and secondary reaction are neglected (see text).

g^{-1}, after which R_2 decreases with increasing S_{sp} ($S_{sp} > 0.3\ m^2\ g^{-1}$). In this way, the C_2 hydrocarbon yield has a maximum at a suitable S_{sp} under these conditions (if reactant pressure drop can be neglected).

Indeed, this tendency is seen in the data obtained over various MgO catalysts (*7, 10*). A similar specific surface area effect has been reported for the C_2 formation from CH_4 pyrolysis (*43*). Strictly speaking, the specific surface area effect is much more pronounced for the calculated result (Fig. 8) than for the actual data (*7, 10*). One reason may be overestimation of the surface dependence with respect to CO_2 formation from $\cdot CH_3$ (Eq. 3) (k_3 is proportional to S_{sp}). Lunsford and colleagues suggest that the C_2 hydrocarbon selectivity would be a function of $1/(S + \text{constant})$ (personal communication, 1987). CO_2 formation may occur by the oxidation of $\cdot CH_3O_2$ in the gas phase. Although there are some other assumptions (reactant pressure drop and secondary reaction are neglected), the specific surface area effect would be qualitatively well explained by the Rideal-redox mechanism where $\cdot CH_3$ coupling occurs in the gas phase. The C_2 hydrocarbon yield decreases with increasing S_{sp} under the condition that O_2 conversion is constant even if the conversion is less than 100%, because R_2/R_1 decreases with increasing S_{sp}.

CONCLUSION

Oxidative coupling of CH_4 over 15% Na^+–MgO can be explained by using the Rideal-redox mechanism, which includes heterogeneous and homogeneous steps. The production of gaseous $\cdot CH_3$, the intermediate, would be a heterogeneous process (surface reaction), and the production of C_2 hydrocarbons, the coupling of $\cdot CH_3$, would be a homogeneous process (gas phase reaction). The activity of the catalyst is related to the rate of oxidation of the surface (k_1) and the rate of reaction between surface oxygen and CH_4 (k_2), and the selectivity is related to the rate ratio of methyl coupling and methyl oxidation (k_4/k_3^2). These constants are easily obtained from the flow experiments. The specific surface area (surface structure) seems to control both the reaction space, where coupling of $\cdot CH_3$ (gas phase reaction k_4) occurs preferably, and the surface, where oxidation of $\cdot CH_3$ to CO_2 (surface reaction k_3) occurs preferably. This method of kinetic analysis can be applied to clarify the catalyst properties of various catalysts, which should be useful in reactor design.

REFERENCES

1. Otsuka, K., and Jinno, K., *Inorg. Chim. Acta* **121,** 237 (1986).
2. Sinev, M. Y., Vorobeva, G. A., and Korchak, V. N., *Kinet. Katal.* **27,** 1164 (1986).
3. Sinev, M. Y., Korchak, V. N., and Krylov, O. V., *in* "Proceedings, 6th Intern. Symp. Heterogeneous Catalysis," Vol. 1, p. 450. Burugarian Acad. Sci., Sofia, 1987.
4. Labinger, J. A., and Ott, K. C., *J. Phys. Chem.* **91,** 2682 (1987).
5. Ali Emesh, I. T., and Amenomiya, Y., *J. Phys. Chem.* **90,** 4785 (1986).
6. Ito, T., Wang, J.-X., Lin, C.-H., and Lunsford, J. H., *J. Amer. Chem. Soc.* **107,** 5062 (1985).
7. Iwamatsu, E., Moriyama, T., Takasaki, N., and Aika, K., *in* "Methane Conversion (Studies in Surface Science and Catalysis, Vol. 36)" (D. M. Bibby *et al.*, Eds.), p. 373. Elsevier, Amsterdam, 1988.
8. Driscoll, J., Martir, W., Wang, J.-X., and Lunsford, J. H., *J. Amer. Chem. Soc.* **107,** 58 (1985).
9. Moriyama, T., Takasaki, N., Iwamatsu, E., and Aika, K., *Chem. Lett.*, 1165 (1986).
10. Iwamatsu, E., Moriyama, T., Takasaki, N., and Aika, K., *J. Chem. Soc. Chem. Commun.*, 19 (1987).
11. Iwamatsu, E., Moriyama, T., Takasaki, N., and Aika, K., *J. Catal.* **113,** 25 (1988).
12. Hinsen, W., and Baerns, M., *Chem. Ztg.* **107,** 223 (1983).
13. Hinsen, W., Bytyn, W., and Baerns, M., *in* "Proceedings, 8th International Congress on Catalysis, Berlin, 1984," Vol. 3, p. 581. Dechema, Frankfurt-am-Main, 1984.
14. Ito, T., and Lunsford, J. H., *Nature (London)* **314,** 721 (1985).
15. Lin, C.-H., Campbell, K. D., Wang, J.-X., and Lunsford, J. H., *J. Phys. Chem.* **90,** 534 (1986).
16. Keller, G. E., and Bhasin, M. M., *J. Catal.* **73,** 9 (1982).
17. Otsuka, K., Jinno, K., and Morikawa, A., *Chem. Lett.*, 499 (1985).

18. Otsuka, K., and Nakajima, T., *Inorg. Chim. Acta* **120,** L27 (1986).
19. Otsuka, K., Liu, Q., and Morikawa, A., *J. Chem. Soc. Chem. Commun.,* 586 (1986).
20. Otsuka, K., Jinno, K., and Morikawa, A., *J. Catal.* **100,** 353 (1986).
21. Otsuka, K., Said, A. A., Jinno, K., and Komatsu, T., *Chem. Lett.,* 77 (1987).
22. Aika, K., Moriyama, T., Takasaki, N., and Iwamatsu, E., *J. Chem. Soc. Chem. Commun.,* 1210 (1986).
23. Aika, K., Moriyama, T., Fujimoto, N., Takasaki, N., and Iwamatsu, E., *in* "Proceedings, 6th Intern. Symp. Heterogeneous Catalysis," Vol. 1, p. 418. Brugarian Acad. Sci., Sofia, 1987.
24. Imai, H., and Tagawa, T., *J. Chem. Soc. Chem. Commun.,* 52 (1986).
25. Matsuura, I., Utsumi, Y., Nakai, M., and Doi, T., *Chem. Lett.,* 1981 (1986).
26. Asami, K., Hashimoto, S., Shikada, T., Fujimoto, K., and Tominaga, H., *Chem. Lett.,* 1233 (1986).
27. Fujimoto, K., Hashimoto, S., Asami, K., and Tominaga, H., *Chem. Lett.* 2157 (1987).
28. Sinev, M., Yu., Korchak, V. N., and Krylov, O. V., *in* "Proceedings, 9th International Congress on Catalysis, Calgary, 1988" (M. J. Phillips and M. Ternan, Eds.), Vol. 3, p. 968. The Chemical Institute of Canada, Ottawa, 1988.
29. Yamagata, N., Tanaka, K., Sakai, S., and Okazaki, S., *Chem. Lett.,* 81 (1987).
30. Sofranko, J. A., Leonard, J. J., and Jones, C. A., *J. Catal.* **103,** 302 (1987).
31. Jones, C. A., Leonard, J. J., and Sofranko, J. A., *J. Catal.* **103,** 311 (1987).
32. Labinger, J. A., Ott, K. C., Mehta, S., Rockstad, H. K., and Zoumalan, S., *J. Chem. Soc. Chem. Commun.,* 543 (1987).
33. Hutchings, G. J., Scurrell, M. S., and Woodhouse, J. R., *J. Chem. Soc. Chem. Commun.,* 1388 (1987).
34. Martin, G.-A., and Mirodatos, C., *J. Chem. Soc. Chem. Commun.,* 1393 (1987).
35. Machida, K., and Enyo, M., *J. Chem. Soc. Chem. Commun.,* 1639 (1987).
36. Roos, J. A., Bakker, A. G., Bosch, H., Van Ommen, J. G., and Ross, J. R. H., *Catal. Today* **1,** 133 (1987).
37. Khachatryan, L. A., Niazyan, O. M., Mantashyan, A. A., Vedeneev, V. I., and Teitel'boim, M. A., *Int. J. Chem. Kinet.* **14,** 1231 (1982).
38. Slagle, I. R., and Gutman, D. J., *J. Amer. Chem. Soc.* **107,** 5342 (1985).
39. Lin, C.-H., Wang, J.-X., and Lunsford, J. H., *J. Catal.* **111,** 302 (1988).
40. Sinev, M. Yu., Korchak, V. N., and Krylov, O. V., *Kinet. Katal.* **28,** 1376 (1987).
41. Aono, K., Fujimoto, N., Iwamatsu, E., and Aika, K., "60th Meeting, Catal. Soc. Japan, Fukuoka, 1987," paper No. 3B06.
42. Aika, K., Isobe, M., Tajima, M., and Onishi, T., *in* "Proceedings, 8th International Congress on Catalysis, Berlin, 1984," Vol. 3, p. 335. Dechema, Frankfurt-am-Main, 1984.
43. van der Zwet, G. P., Hendriks, P. A. J. M., and van Santen, R. A., presented at the Symposium "European Workshop on Catalytic Methane Conversion," 1988, Bochum, FRG.